Improved Predictive Torque Control with Unidirectional Voltage Vector Selection of PMSM fed by Three-Level Neutral-Point-Clamped Inverter

Ibrahim Mohd Alsofyani1 and Kyo-Beum Lee[2]
[1] Digital Center, SEMI-TS, Sengnam-Si, Korea
[2] Department of Electrical and Computer Engineering, Ajou University, Suwon, 16499, Korea

***Abstract*-- This paper proposes an improved predictive toque control with unidirectional voltage vector selection method for a three-level neutral-point-clamped inverter (3L-NPCI) fed permanent magnet synchronous motor. The proposed algorithm can restrict the candidate voltage vectors (VVs) within 60º of the space voltage diagram (SVD), which are the nearest to the flux trajectory for each 60º flux sector. After the subdivision of the SVD and flux trajectory, the proposed method can keep VVs in one direction during the prediction process which can result in significant torque/flux reduction. Therefore, the proposed algorithm achieves superior performance to the conventional method which requires enumerating all 19 voltage vectors while significantly reducing the computational burden. The proposed FCS-PTC of PMSM has also other advantages, such as improved capacitance voltages balancing, small computation time due to the reduced number of admissible voltage vectors considered in the cost function, and easy implementation. The effectiveness of the proposed method is verified through simulation and experimental results.**

***Index Terms*--The authors shall provide up to 4 keywords or phrases (in alphabetical order and separated by commas) to help identify the major topics of the paper.**

I. Introduction

Over the years, finite control set model predictive control (FCS-MPC) becomes widely applied for high performance AC machines owing to its distinguished merits such as easy inclusion of non-linear constraints, simple implementation, intuitive concept, and robust control. In this method, the discrete model of motor is used to predict the motor variables based on tracking the reference signals is constructed to obtain the optimal voltage vector (VV) using a cost function, so as to achieve the optimal control performance [1]-[6]. It is categorized as FCS-predictive current control (FCS-PCC) and FCS-predictive torque control (FCS-PTC). However, this algorithm still suffers from drawbacks such as the increased computation load for multilevel converters owing to large number of admissible VVs.

The three-level neutral-point-clamped (3L-NPC) inverters is a widely implemented multilevel converter in industries owing to the merits of less total harmonic distortion (THD), higher efficiency, and less switching pressure across switching systems [7]-[8]. Yet, designing an FCS-MPC of AC machine fed by 3L-NPC inverter requires 19 different voltage vectors by 27 switching states to be evaluated by the cost function for every sampling period resulting in high computation burden [9]-[12]. There are some studies which can be categorized under deadbeat control and lookup table methods to reduce the computation load [13]-[17]. The deadbeat control method is very complicated for FCS-PTC since it requires the derivation of voltage reference based on the flux and torque. In the deadbeat control, the optimum location of space vector diagram sector is determined by a reference voltage. However, the reference voltage is used to determine the sector or sub-sector of the space vector diagram where the voltage vectors in the selected sector or subsector need to be evaluated in the cost function. Therefore, even if the reference voltage vector is determined, it is still needed to define the closest voltage vectors to be evaluated by the cost function. However, the performance of FCS-PTC using predefined VV switching tables is much easier, and it depends on the structure and operating circumstances.

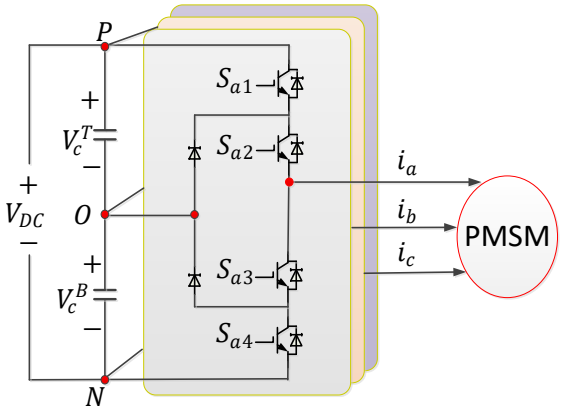

Fig. 1. Configuration of the 3L-NPCI.

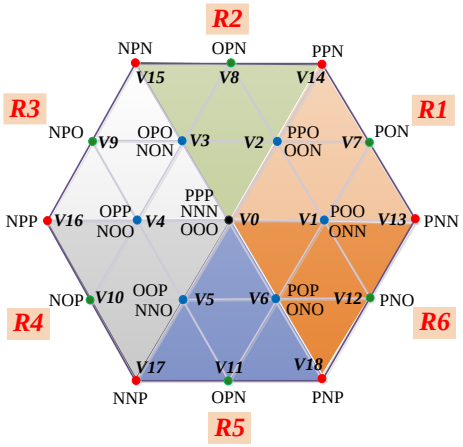

Fig. 2. Space-vector diagram of a three-level inverter.

This paper proposes a new and simplified VV selection approach for improving the performance of FCS-MPTC of 3L-NPC inverter fed permanent magnet synchronous motor (PMSM). This method contributes to reduce the number of admissible VVs greatly and effectively. Unlike previous research works, the number of enumerations of VVs is reduced from 19 to 6 per control cycle, which contributes to significant reduction of computation time. Furthermore, this paper proposed a simple balancing method for the capacitive voltages without and need for a weighting factor. The proposed method can achieve superior performance to the original conventional algorithm enumerating the 19 VVs. The effectiveness of the proposed PTC method is verified through simulation and experimental results.

II. Fundamentals of 3L-NPC

Fig. 1 shows the configuration of PMSM fed 3L- NPCI inverter. Each leg of 3L- NPCI has four switching devices: S_{x1}, S_{x2}, S_{x3}, and S_{x4} $(x = a, b, \text{and } c)$. As can be depicted in the voltage vector diagram (VVD) of the 3L-NPCI shown in Fig. 2, there are 19 various voltage vectors (VVs) with a grouping of 27 switching states (SSs). This includes three zero VV (ZVV) ***V0***, 6 small VVs (SVVs) ***V1***, . . . ***V6***, 6 medium VVs (MVVs) ***V7***, . . . ***V12***, and 6 large VVs (LVVs) ***V13***, . . . ***V18***. Depending on the connections to the top capacitor voltage (V_c^T), bottom capacitor voltage (V_c^B) or neutral point (NP), ZVV has three SSs, SVV has two opposite SSs, and MVVs has a single SS. *P*, *O*, and *N* indicate the phase connections to '+' DC voltage bus, NP, and '–' DC bus, respectively. In order to ensure a balanced 3L-NPCI drive system, the voltages for top and bottom capacitors should be evenly distributed.

III. Basics of FCS-PTC fed by 3L-NPC

The discrete expressions for the FS-MPTC of PMSM in the stationary reference frame are given as follows:

$$\vec{\lambda}_s(\mathrm{k}) = L_s \cdot \vec{\imath}_s(k) + \vec{\lambda}_{pm}(k) \quad (1)$$

$$T_e = \frac{3}{2} p \cdot (\ \vec{\lambda}_s(\mathrm{k}) \cdot \vec{\imath}_s(k)) \quad (2)$$

where $\vec{\imath}_s$, and $\vec{\lambda}_s$ are the stator current, and stator flux vectors. $\vec{\lambda}_{pm}$ is the permanent magnet flux. T_e is the electrical motor torque. R_s and L_s are the stator resistance and stator self-inductance, respectively. P is the number of pole pairs.

The predicted quantities of stator flux vector and stator current vectors can be expressed as

$$\vec{\lambda}_s(k+1) = \vec{\lambda}_s(\mathrm{k}) + T_s \cdot \vec{v}_s(k) + T_s R_s \cdot \vec{\imath}_s(k) + T_s \cdot Y \cdot \omega_r(k), \quad (3)$$

$$\vec{\imath}_s(k+1) = \Lambda \cdot \vec{\imath}_s(k) + M \cdot \vec{v}_s(k) + \Gamma, \quad (4)$$

where

$$\vec{\imath}_s = \begin{bmatrix} i_{s\alpha} \\ i_{s\beta} \end{bmatrix}, \quad \vec{v}_s = \begin{bmatrix} v_{s\alpha} \\ v_{s\beta} \end{bmatrix}, \quad Y = \begin{bmatrix} \psi_{s\beta} \\ -\psi_{s\alpha} \end{bmatrix},$$

$$\Lambda = \begin{bmatrix} 1 - R_s \cdot T_s/L_s & L_s \cdot T_s \cdot \omega_r(k) \\ -L_s . T_s \cdot \omega_r(k) & 1 - R_s \cdot T_s/L_s \end{bmatrix}$$

$$M = \begin{bmatrix} T_s/L_s & 0 \\ 0 & T_s/L_s \end{bmatrix}, \quad \Gamma = \begin{bmatrix} 0 \\ -\vec{\lambda}_{pm} \cdot \omega_r \cdot T_s/L_s \end{bmatrix}$$

where $\vec{v}_s$ is the stator VV and ω_r is the rotor speed. T_s is the sampling time. k and $k+1$ indicate the present and predicted control discrete cycles, respectively.

Depending on the predicted values on (3) and (4), the electric torque can be predicted as below:

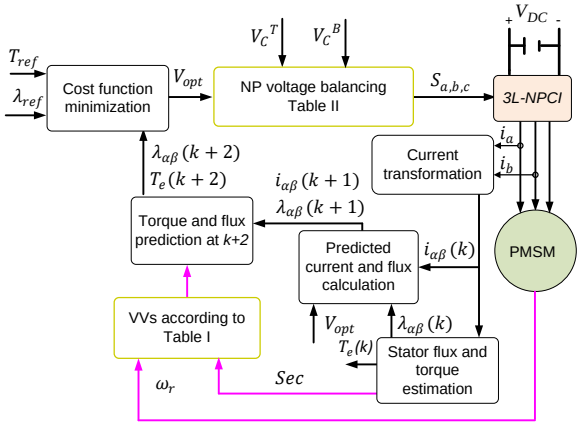

Fig. 3. Proposed FCS-PTC of PMSM fed by 3L-NPCI.

$$T_e(k+1) = \frac{3}{2} p . \Big(\vec{\lambda}_s(k+1) \cdot \vec{\imath}_s(k+1) \Big), \quad (5)$$

As previously mentioned, the 3L-NPCI structure consists of 19 VVs. To determine the optimal VV among the admissible VVs, a cost function is formed as:

$$g = \left| T_{ref} - T_e(k+1) \right| + W_\psi \left| \lambda_{ref} - \left| \vec{\psi}_s(k+1) \right| \right|, \quad (6)$$

where T_{ref} is a torque reference, and λ_{ref} is the flux reference at the k^{th} sampling time. W_ψ is the weighting factor that identifies the relative value of the flux control objective.

TABLE I
OPTIMAL VVs FOR EACH FLUX SECTOR.

Flux sector	Optimal VVs	
	Forward Motor Direction	Reverse Motor Direction
Sec (1)	[***V0***, ***V2***, ***V3***, ***V8***, ***V14***, and ***V15***]	[***V0***, ***V5***, ***V6***, ***V11***, ***V17***, and ***V18***]
Sec (2)	[***V0***, ***V3***, ***V4***, ***V9***, ***V15***, and ***V16***]	[***V0***, ***V1***, ***V6***, ***V12***, ***V13***, and ***V18***]
Sec (3)	[***V0***, ***V4***, ***V5***, ***V10***, ***V16***, and ***V17***]	[***V0***, ***V1***, ***V2***, ***V7***, ***V13***, and ***V14***]
Sec (4)	[***V0***, ***V5***, ***V6***, ***V11***, ***V17***, and ***V18***]	[***V0***, ***V2***, ***V3***, ***V8***, ***V14***, and ***V15***]
Sec (5)	[***V0***, ***V1***, ***V6***, ***V12***, ***V13***, and ***V18***]	[***V0***, ***V3***, ***V4***, ***V9***, ***V15***, and ***V16***]
Sec (6)	[***V0***, ***V1***, ***V2***, ***V7***, ***V13***, and ***V14***]	[***V0***, ***V4***, ***V5***, ***V10***, ***V16***, and ***V17***]

TABLE II
OPTIMAL SSs OF SVVs FOR CAPACITANCE VOLTAGE BALANCING.

	V_{opt} ***(V1)***	V_{opt} ***(V2)***	V_{opt} ***(V3)***	V_{opt} ***(V4)***	V_{opt} ***(V5)***	V_{opt} ***(V6)***
$V_c^T \geq V_c^B$	[POO]	[PPO]	[OPO]	[OPP]	[OOP]	[POP]
$V_c^T < V_c^B$	[ONN]	[OON]	[NON]	[NOO]	[NNO]	[ONO]

IV. PROPOSED FCS-PTC

The structure of the proposed FCS-MPTC is shown in Fig. 3. It can be seen the proposed method still uses the same stages of estimation, prediction, and cost function evaluation as in the classical PTC. The main purpose of the proposed PTC method is to improve the performance of the FCS-MPTC method for 3L-NPC inverter system while reducing the number of admissible VVs; thus, reducing the computation load on the DSP. The flux trajectory is divided into six sectors. As the position of the stator flux, ϕ_s, is estimated as

$$\phi_s = \arctan(\lambda_\beta / \lambda_\alpha) \quad (7)$$

Therefore, the $\alpha - \beta$ plane of flux rotation can be determined by

$$(2N-3)\cdot\pi/6 \leq Sec(N) \leq (2N-1)\cdot\pi/6 \quad (8)$$

where Sec is the flux sector and $N = 1, \ldots, 6$.

The optimum directions of active VVs that ensures the circular motion of stator flux according to the flux position should be determined.

TABLE III
PMSM Parameters

Parameter	Value
Torque rating	60 Nm
Power rating	11 kW
Current rating	19.9 A
Speed rating	1750 rpm
Permanent magnet flux	0.554 Wb
Number of poles	6
Stator resistance	0.349 Ω
Stator inductance	15.6 mH

By neglecting the stator resistance, the change in stator flux vector $\Delta\psi_s$ can be expressed as [2]:

$$\Delta\psi_s = v_s \, T_s \quad (9)$$

Hence, it is obvious that the variation in stator flux $\Delta\psi_s$ is controlled by the VV and hence is proportional to the direction of the applied VV during T_s. Like the segmentation of the flux trajectory, the VSVD for the 3L-NPCI is also divided into six symmetrical regions (i.e. *R1 – R6*) as shown in Fig. 2.

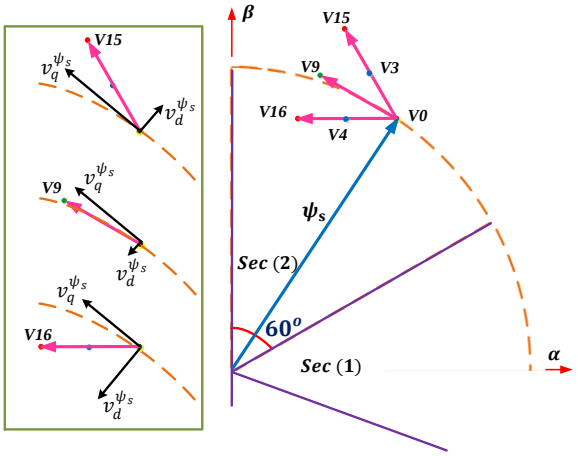

Fig. 4. Illustration for the optimal candidate VVs for Sec (2).

In this way, each flux sector will correspond to one SVD region, which contains the nearest VVs to the circular flux trajectory as shown in Fig. 4.

Fig. 4. Illustrates an example when the stator flux λ_s is located at Sec (2). The VSVD region *R3* is the optimum region in the anticlockwise direction and the region $R6$ is the optimal VSVD region in the clockwise direction. For convenience, Table I shows the optimum VSVD region for each flux sector. Unlike previous works, in order to restrict the VVs in one direction, this paper proposes the motor speed ω_r for both VVs prediction selection, because the rotor speed and flux rotation travels in the same direction [4]. In this way, the predicted VVs will be restricted in one direction and the torque and flux can vary within the VVs in the selected SVD region as shown in Fig. 5b. Assuming the space vector of the stator

flux linkage moving anticlockwise at $Sec(2)$, according to Table I the candidate voltage vectors in SVD region R3 [***V0***, ***V3***, ***V4***, ***V9***, ***V15***, and ***V16***] are used for controlling the flux and torque. Notably, the radial VV component ($v_d^{\psi_s}$) and tangential VV component ($v_q^{\psi_s}$) for some candidate VVs (which are perpendicular and tangential to the trajectory of the stator flux) are analyzed for the same flux position. The radial voltage component is responsible for the increase and decrease of flux while the tangential voltage component is responsible of increasing and

decreasing the torque. By inspecting three candidate VVs (***V9***, ***V15***, and ***V16***) for R3, it is clearly seen that all of the tangential components of these voltages are pointing in the anticlockwise direction, which can result in the increase of torque. As for the reduction of torque, the SVVs (***V3***, ***V4***) or ZVV (***V0***) can be used in the prediction process. Additionally, it apparent that the radial component for ***V15*** is greater than the flux reference whereas the radial component for ***V16*** is less than the flux reference. Hence, the VVs in the optimal SVD zone can satisfy the increase and decrease in the stator flux and torque. This can be also applied to the SVVs (***V3***, ***V4***).

In this paper, to ensure balanced dc-link capacitor voltages without a need for additional weighting factor, the opposite SSs of the SVVs are proposed as in Table II. In this way, the control complexity owing to tedious tuning of weighting factors is reduced.

V. Results

The performance of the proposed PTC for the 3L-NPCI -fed PMSM was simulated using PSIM software package. The proposed method is also compared with the conventional FCS-PTC for 3L-NPC inverter with 19 VVs. As previously mentioned, the proposed method only requires 6 out of 19 VVs per control cycle. The specifications of PMSM motor is provided in Table III. Both PTC methods are tested with the same sampling period of 100 μs and same weighting factor.

Fig. 5 shows a step change of torque from 5 to 50 Nm is applied during speed operation of 400 rpm at 0.15 s. It can be observed that the proposed PTC can achieve excellent performance in terms of flux, torque, and current ripple reduction for both torque references when compared the conventional PTC. Additionally, the proposed PTC shows very good balanced capacitance voltages throughout the operation. Nevertheless, it can be observed that capacitor voltages for the conventional PTC is largely deviated after the torque is stepped up to 50 Nm mainly due to the VVs selections. It is worth noting that the switching states for the small VVs applied to the inverter are generated according to Table II to balance the capacitor voltages. It can be noted from the zoomed regions A and B of proposed PTC that the optimal VVs are smoothly selected depending on the flux sector according to Table I. For example, ***V0***, ***V4***, and ***V5*** are the optimal VVs corresponding to flux sector 3, whereas ***V0***, ***V5***, ***V6*** are the optimal VVs corresponding to flux *Sec* (4). Since the optimal VVs are mainly from SVVs, the balancing of capacitor voltages can be obtained according to Table II.

By comparing the zoomed regions C and D for the conventional PTC, it can be observed that the VVs in region C contain higher number of small VVs compared to region D. Hence, this is the reason why the capacitor voltages become deviated after the step change of torque to 50 Nm.

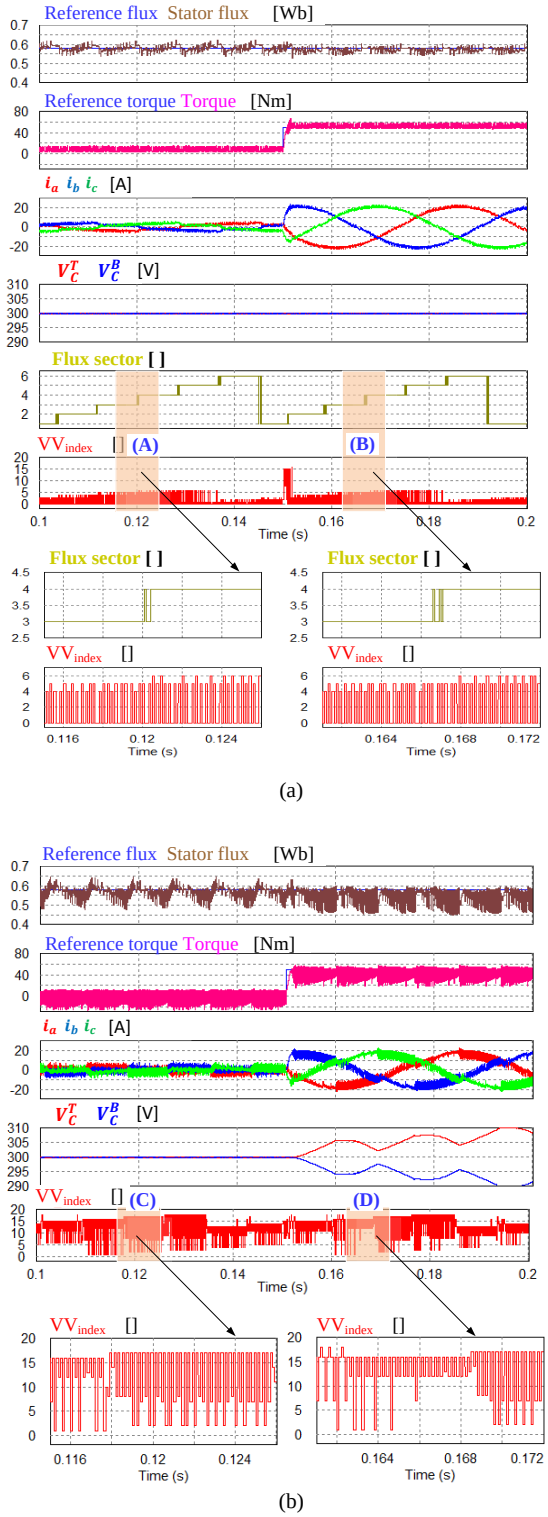

(a)

(b)

Fig. 5. Simulation results for (a) Proposed PTC and (b) Conventional PTC.

Figure 6 displays the experimental steady-state performance at 100 rpm with a load of 10 Nm for the proposed and conventional PTCs. The waveforms in Fig. 6 are flux, torque, capacitor voltage error ($V_{c.err}$), line-to-line voltage V_{ab}, and output current in A-phase i_a.

Where $V_{c.err}$ is calculated from top and capacitor voltages as ,

$$V_{c.err} = V_c^T - V_c^B \tag{10}$$

It is clearly observed that the proposed PTC has excellent perforamnce in terms of current, flux, and torqe ripple reduction when compared to conventioanl PTC. Additionally, the proopsed PTC has stable and balanced capacitance voltage throughtout the operation with nice line to line voltage waveform .

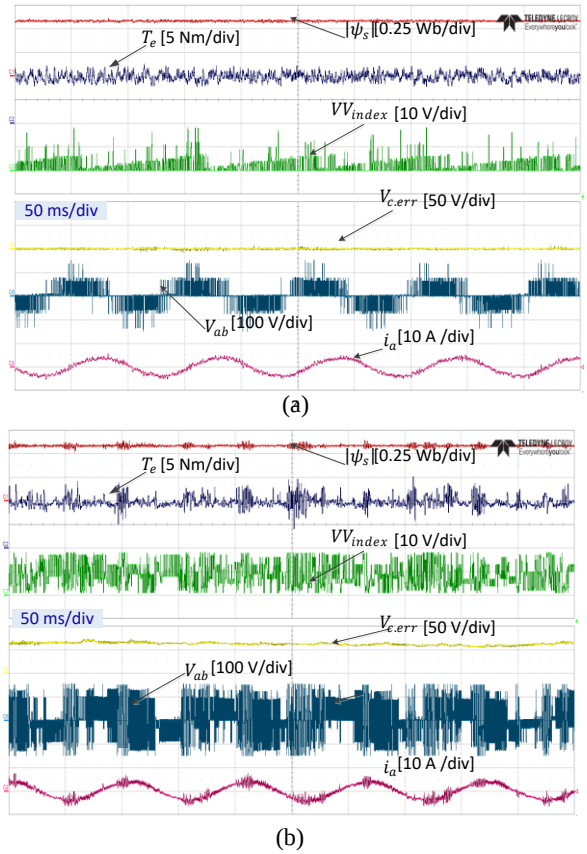

Fig. 6. Experimental results for (a) Proposed PTC and (b) Conventional PTC.

VI. Conclusion

This paper proposed an improved predictive torque control method with unidirectional VV selection for PMSM fed the 3L-NPC system. The simulation and experimental results of proposed method showed excellent steady state performance compared to the conventional method with 19 VVs. The proposed method was simply designed to minimize the number of VVs in the multilevel converters using speed and flux information with a simple lookup table. In addition, the problem of capacitor voltage deviation in 3L-NPCI system was simply solved without applying addition weighting factors. The effectiveness of the proposed technique was proved through the simulation and experimental results.

Acknowledgment

Please place an eventual Acknowledgment here, before the References. Put sponsor acknowledgments in an unnumbered footnote on the first page.

References

[1] B. Cao, B. M. Grainger, X. Wang, Y. Zou, G. F. Reed and Z. -H. Mao, "Direct Torque Model Predictive Control of a Five-Phase Permanent Magnet Synchronous Motor," *IEEE Trans. Power Electron*., vol. 36, no. 2, pp. 2346-2360, Feb. 2021.

[2] I. M. Alsofyani and K. -B. Lee, "A Unidirectional Voltage Vector Preselection Strategy for Optimizing Model Predictive Torque Control With Discrete Space Vector Modulation of IPMSM," in *IEEE Transactions on Industrial Electronics*, vol. 69, no. 12, pp. 12305-12315, Dec. 2022.

[3] P. Correa, M. Pacas and J. Rodriguez, "Predictive Torque Control for Inverter-Fed Induction Machines," *IEEE Trans. Ind. Electron.*, vol. 54, no. 2, pp. 1073-1079, Apr. 2007.

[4] H. Iqbal, et al., Model predictive control of Packed U-Cell inverter for microgrid applications,. *Energy Reports*, 2022, 8, 813-830.

[5] S. Kouro, P. Cortes, R. Vargas, U. Ammann and J. Rodriguez, "Model Predictive Control—A Simple and Powerful Method to Control Power Converters," *IEEE Trans. Ind. Electron*., vol. 56, no. 6, pp. 1826-1838, Jun. 2009.

[6] S. A. Q. Mohammed, I. M. Alsofyani and K. -B. Lee, "Improved Adaptive CCS-MPCC for Distorted Model Parameters Mitigation of IPMSM Drives," *IEEE Trans. Ind. Electron*., early access, doi: 10.1109/TIE.2023.3279550.

[7] L. M. Halabi, I. M. Alsofyani and K. -B. Lee, "Multi Open-/Short-Circuit Fault-Tolerance Using Modified SVM Technique for Three-Level HANPC Converters," *IEEE Trans. Power Electron*., vol. 36, no. 12, pp. 13621-13633, Dec. 2021.

[8] Zhang, G.; Su, Y.; Zhou, Z.; Geng, Q. A Carrier-Based Discontinuous PWM Strategy of NPC Three-Level Inverter for Common-Mode Voltage and Switching Loss Reduction. *Electronics* 2021, 10, 3041.

[9] M. Habibullah, D. D. C. Lu, D. Xiao, and M. F. Rahman, "Finite-state predictive torque control of induction motor supplied from a three-level NPC voltage source inverter," IEEE Trans. Power Electron., vol. 32, no. 1, pp. 479–489, Jan. 2017.

[10] F. Donoso, A. Mora, R. Cardenas, A. Angulo, D. Saez, and M. Rivera, "Finite-setmodel-predictive control strategies for a 3L-NPC inverter operating with fixed switching frequency," *IEEE Trans. Ind. Electron.*, vol. 65, no. 5, pp. 3954–3965, May 2018.

[11] Z. Zhang, Z. Li, M. P. Kazmierkowski, J. Rodríguez and R. Kennel, "Robust predictive control of three-level NPC back-to-back power converter PMSG wind turbine systems with revised predictions," *IEEE Trans. Power Electron.*, vol. 33, no. 11, pp. 9588–9598, Nov. 2018.

[12] S. Xu, Z. Sun, C. Yao, H. Zhang, W. Hua and G. Ma, "Model predictive control with constant switching frequency for three-level T-type inverter fed PMSM drives," *IEEE Trans. Ind. Electron*., vol. 69, no. 9, pp. 8839-8850, Sept. 2022.

[13] I. Osman, D. Xiao, M. F. Rahman, M. Norambuena, and J. Rodriguez, “An optimal reduced-control-set model predictive flux control for 3L-NPC fed induction motor drive,” *IEEE Trans. Energy Convers*., vol. 36, no. 4, pp. 2967-2976, Dec. 2021.

[14] C. Xia, T. Liu, T. Shi, and Z. Song, “A simplified finite-control-set model-predictive control for power converters,” *IEEE Trans. Ind. Inform*., vol. 10, no. 2, pp. 991-1002, May. 2014.

[15] J. Rodriguez et al., “Latest advances of model predictive control in electrical drives. Part I: Basic concepts and advanced strategies,” *IEEE Trans. Power Electron*., vo. 37, no. 4, pp. 3927-3942, Apr. 2022.

[16] M. S. R. Saeed, W. Song, B. Yu and X. Wu, "Low-Complexity Deadbeat Model Predictive Current Control With Duty Ratio for Five-Phase PMSM Drives," IEEE Transactions on Power Electronics, vol. 35, no. 11, pp. 12085-12099, Nov. 2020.

[17] Y. Yao, Y. Huang, F. Peng, J. Dong, and H. Zhang, “An improved Deadbeat Predictive Current Control with Online Parameter Identification for Surface-Mounted PMSMs,” *IEEE Transactions on Industrial Electronics*, vol. 67, no. 12, pp. 10 145–10 155, 2019.